JOURNAL OF COMPUTATIONAL PHYSICS 71, 371–390 (1987)

A Two-Dimensional Finite Element Multigroup Diffusion Theory for Neutral Atom Transport in Plasmas

MOHAMMAD Z. HASAN AND ROBERT W. CONN

Mechanical, Aerospace, and Nuclear Engineering Department, Center for Plasma Physics and Fusion Engineering, University of California, Los Angeles, Los Angeles, California 90024

Received May 23, 1986; revised November 12, 1986

Solution of the energy-dependent diffusion equation in two dimensions is formulated by multigroup approximation of the energy variable and general triangular mesh, finite element discretization of the spatial domain. Finite element formulation is done by Galerkin's method. Based on this formulation, a two-dimensional multigroup finite element diffusion theory code, FENAT, has been developed for the transport of neutral atoms in fusion plasmas. FENAT solves the multigroup diffusion equation in X–Y cartesian and R–Z cylindrical/toroidal geometries. Use of the finite element method allows solution of problems in which the plasma cross section has an arbitrary shape. The accuracy of FENAT has been verified by comparing results to those obtained using the two-dimensional discrete ordinate transport theory code, DOT-4.3. Results of application of FENAT to the transport of limiter-originated neutral atoms in a tokamak fusion machine are presented.

I. INTRODUCTION

The importance of the neutral atom distribution in a fusion plasma is well recognized [1, 2]. Neutral atoms influence the plasma particle and energy balance by undergoing ionization and charge-exchange reactions in the plasma and by introducing high-Z impurity atoms through processes such as sputtering and impact desorption. Neutral atom sputtering of limiter or divertor components and vacuum vessel wall in a fusion device affect the lifetime of these components, in addition to the problem of impurity production and plasma contamination. Also, knowledge of the energy spectrum of neutral atoms emerging from the plasma is useful for diagnostic purposes, such as in the determination of the plasma ion temperature. Fluid plasma codes used to describe plasma behavior in tokamaks, such as WHIST [3] or BALDUR [4], employ the results of neutral calculations as input to the plasma simulation. For all these reasons, the accurate and efficient description of neutral atom transport in complex geometries is a key problem in fusion research.

In general, neutral atom transport must be solved numerically because of the

0021-9991/87 $3.00

nonhomogeneity or spatial variation of the plasma temperature and density. Several numerical solutions in one-dimensional geometry are available. Burrell [5] developed the code, NEUCG, based on the solution of an integral equation for a one-dimensional cylindrical plasma. Audenaerde *et al.* [6] developed the one-dimensional slab geometry code, SPUDNUT, based on the numerical solution of an integral equation for the charge-exchange collision density. Hughes and Post [7] wrote a one-dimensional cylindrical geometry code for neutral atom transport using the Monte Carlo method. Duchs *et al.* [8] solved for the neutral atom distribution in one-dimensional cylindrical plasma using a charge-exchange generation method, allowing up to 10 successive generations of charge-exchange neutrals. Garcia *et al.* [9] numerically solved for the neutral atom distribution in a one-dimensional slab plasma and in a half space using the F_N-method.

Neutral atom distribution in multidimensional plasma geometries have been obtained using the Monte Carlo methods. Heifetz *et al.* [10] and Reiter and Nicolai [11] have reported multidimensional Monte Carlo codes for neutral atom transport. Codes written specifically for neutron transport, such a ANISN [12], DOT-4.3 [13], and TRIDENT [14], can be used to calculate the distribution of neutral atoms in plasmas. Application of ANISN is reported in reference [15].

Often, a one-dimensional approximation of the fusion plasma is not realistic because there are localized sources of neutrals or because the geometry is not readily simplified. We have shown elsewhere [16, 17] that energy-dependent diffusion theory with P_1-Marshak boundary conditions provides very good accuracy for the transport of neutral atoms in fusion plasmas. A two-dimensional diffusion theory code for the transport of neutral atoms will be much faster than deterministic transport or Monte Carlo codes. Therefore, the code FENAT has been developed based on the finite element solution of the energy-dependent diffusion equation in X–Y cartesian and R–Z cylindrical/toroidal geometries. The energy dependence is treated by the multigroup method. In Section II, the multigroup diffusion equation is written in (x, y, Ψ) toroidal coordinates. Finite element formulation of the solution by Galerkin's method is treated in Section III, and the solution of the resulting system of algebraic equations and the characteristics of the code, FENAT, are presented in Section IV. Section V contains verification of the accuracy of FENAT and the results of sample calculations for neutral atom transport in the TEXTOR tokamak [18].

II. Diffusion Equation in Toroidal Geometry

The steady state energy and space-dependent diffusion equation for neutral atom transport is

$$-\nabla \cdot D(\mathbf{r}, E)\, \nabla\phi(\mathbf{r}, E) + \sigma_t(\mathbf{r}, E)\, \phi(\mathbf{r}, E)$$

$$\int \partial E' \sigma_{cx}(\mathbf{r}, E' \to E)\, \phi(\mathbf{r}, E') + S_v(\mathbf{r}, E), \tag{1}$$

where $\phi(\mathbf{r}, E)$ is the total neutral atom flux, $D(\mathbf{r}, E)$ is the diffusion coefficient, $\sigma_t(\mathbf{r}, E)$ is the total plasma-neutral interaction cross section (ionization plus charge exchange), $\sigma_{cx}(\mathbf{r}, E' \to E)$ is the charge exchange cross section where a neutral atom with energy E' charge exchanges with a plasma ion of energy E, and $S_v(\mathbf{r}, E)$ is the volumetric source of neutral atoms. A common volumetric source would be the recombination source which is important in high density plasma. Treating the energy dependence by the multigroup method, the group diffusion equation corresponding ot Eq. (1) becomes [19, 20]

$$-\nabla \cdot D_g(\mathbf{r})\,\nabla\phi_g(\mathbf{r}) + \sigma_{t,g}(\mathbf{r})\,\phi_g(\mathbf{r}) = \sum_{g'=1}^{G} \sigma_{g' \to g}(\mathbf{r})\,\phi_{g'}(\mathbf{r}) + S_{v,g}(\mathbf{r}) \qquad g = 1, 2, \ldots, G, \tag{2}$$

where g denotes a particular energy group. For P_1-diffusion theory with isotropic charge exchange (scattering) cross section, the diffusion coefficient D_g is given by $1/3\sigma_{t,g}$. In Eq. (2), $\sigma_{g' \to g}$ is the group to group charge exchange cross section. Evaluation of these group cross sections is discussed in [21]. The multigroup cross sections used here are calculated by the code PLASMX [21]. Equation (2) reresents a set of G partial differential equations coupled by the first term in the right-hand side.

Equation (2) is valid for any coordinate system provided proper expressions are used for the gradient and divergence terms. This equation will now be written in the toroidal coordinate system (x, y, Ψ) shown in Fig. 1. The metric (h_1, h_2, h_3) of this system is given by $h_1 = h_2 = 1$ and $h_3 = (R + x)$. Gradient and divergence terms in this system are [22]

$$\nabla A = \frac{1}{h_1}\frac{\partial A}{\partial x}\hat{x} + \frac{1}{h_2}\frac{\partial A}{\partial y}\hat{y} + \frac{1}{h_3}\frac{\partial A}{\partial \Psi}\hat{\Psi}$$

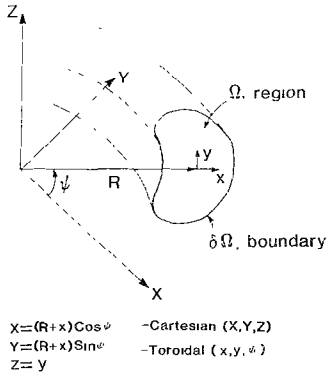

FIG. 1. Toroidal coordinates (x, y, Ψ).

and

$$\nabla \cdot \mathbf{B} = \frac{1}{h_1 h_2 h_3}\left[\frac{\partial}{\partial x}\left(\frac{h_2 h_3}{h_1}\frac{\partial B}{\partial x}\right)+\frac{\partial}{\partial y}\left(\frac{h_3 h_1}{h_2}\frac{\partial B}{\partial y}\right)+\frac{\partial}{\partial \Psi}\left(\frac{h_1 h_2}{h_3}\frac{\partial B}{\partial \Psi}\right)\right],$$

where $\hat{x}$, $\hat{y}$, and $\hat{\Psi}$ are the unit vectors in the respective directions of the toroidal coordinates (x, y, Ψ). Using these expressions in Eq. (2), with $A = \phi_g$ and $\mathbf{B} = D_g \nabla \phi_g$, the group diffusion equation in toroidal coordinates (x, y, Ψ) becomes

$$\begin{aligned} &-\frac{1}{(R+x)}\frac{\partial}{\partial x}(R+x)\, D_g \frac{\partial \phi_g}{\partial x} - \frac{1}{(R+x)}\frac{\partial}{\partial y}(R+x)\, D_g \frac{\partial \phi_g}{\partial y} \\ &\quad -\frac{1}{(R+x)^2}\frac{\partial}{\partial \Psi}(R+x)\, D_g \frac{\partial \phi_g}{\partial \Psi} + \sigma_{t,g}\phi_g \\ &\quad = \sum_{g'=1}^{G} \sigma_{g' \to g}\phi_{g'} + S_{v,g}. \end{aligned} \tag{3}$$

When written in the toroidal coordinates (r, θ, Ψ), where $x = r\cos\theta$ and $y = r\sin\theta$, Eq. (3) becomes the same as that obtained by Pomraning and Stevens [23] by first writing the transport equation in (r, θ, Ψ) and then taking the P_1 approximation of the angular flux to derive the P_1 diffusion equation.

With toroidal symmetry (i.e., Ψ-symmetry), Eq. (3) becomes

$$\begin{aligned} &-\frac{1}{(R+x)}\frac{\partial}{\partial x}(R+x)\, D_g \frac{\partial \phi_g}{\partial x} - \frac{\partial}{\partial y} D_g \frac{\partial \phi_g}{\partial y} + \sigma_{t,g}\phi_g \\ &\quad = \sum_{g'=1}^{G} \sigma_{g' \to g}\phi_{g'} + S_{v,g}, \end{aligned} \tag{4}$$

in domain Ω. Without the factor $(R+x)$ Eq. (4) is the group diffusion equation in X–Y Cartesian coordinates, and with $(R+x)$ replaced by R and y by Z, it becomes the group diffusion equation in R–Z cylindrical coordinates. The boundary conditions considered for Eq. (4) can be written as

$$J^g_{\text{in}} = S^g_0 + \alpha^g J^g_{\text{out}}, \tag{5}$$

where J_{in} and J_{out} are the scalar current of neutral atoms at the surface, S_0 is the surface source and α is the reflection coefficient for the neutral atoms from the wall material. Using the P_1-Marshak expressions for J_{in} and J_{out} in Eq. (5) [20], the boundary conditions can be written after some algebra, as

$$D\frac{\partial \phi_s}{\partial n} = \left(\frac{1-\alpha}{1+\alpha}\right)\frac{\phi_s}{2} - \frac{2S_0}{(1+\alpha)}, \tag{6}$$

valid on $\partial\Omega$, the boundary of the domain Ω. In Eq. (6), $\partial\phi_s/\partial n$ is the normal

derivative of neutral atom flux at the surface. Special cases included in Eq. (6) are free-surface boundary conditions ($\alpha = 0$), reflection conditions ($\alpha = 1$), and general albedo boundary conditions (α neither 0 nor 1). If there is no boundary source, $S_0 = 0$.

III. Galerkin Formulation of Solution

Finite element solution of Eqs. (4) and (6) is formulated by Galerkin's method. Since the diffusion equation is self-adjoint, formulation by the variational method will result in the same equations as by Galerkin formulation. The group diffusion equation can be written in operator notation as

$$L\phi_g = q_g \tag{7}$$

where,

$$L \equiv -\mathbf{V} \cdot D_g \mathbf{V} + \sigma_{t,g}$$

and

$$q_g \equiv \sum_{g'=1}^{G} \sigma_{g' \to g} \phi_{g'} + S_{v,g}.$$

For clarity, the subscript or superscript "g" will be dropped from now on except where ambiguity may arise. Let the neutral flux, ϕ, be approximated as

$$\phi \simeq [N]\{\Phi\} \tag{8}$$

where,

$[N]$ = row vector of suitably choosen basis functions (functions of the spatial coordinates) and

$\{\Phi\}$ = column vector of unknown flux (nodal) values.

In the Galerkin formulation, the weak form of Eq. (7) is [24]

$$\int_\Omega [N]^{\mathrm{T}}(L\phi - q)\, dV = 0$$

or

$$-\int_\Omega [N]^{\mathrm{T}} \mathbf{V} \cdot (D\mathbf{V}\phi)\, dV + \int_\Omega [N]^{\mathrm{T}} \sigma_t \phi\, dV - \int_\Omega [N]^{\mathrm{T}} \left\{ \sum_{g'=1}^{G} \sigma_{g' \to g} \phi_{g'} + S_v \right\} dV = 0,$$

where $[N]^{\mathrm{T}}$ is the transpose of $[N]$. The first term of the above equation can be

simplified by using vector identity and Gauss' divergence theorem [17]. When this is done, the above equation becomes

$$\int_{\Omega} \nabla[N]^{\mathrm{T}} \cdot D\nabla\phi \, dV - \int_{\partial\Omega} [N]^{\mathrm{T}} D \frac{\partial \phi_s}{\partial n} \, dS + \int_{\Omega} [N]^{\mathrm{T}} \sigma_t \phi \, dV - \int_{\Omega} [N]^{\mathrm{T}} \left\{ \sum_{g'=1}^{G} \sigma_{g' \to g} \phi_{g'} + S_v \right\} dV = 0. \tag{9}$$

In two dimensions, the basis functions, N, are functions of x and y. Therefore, from Eq. (8),

$$\frac{\partial \phi}{\partial x} = \frac{\partial [N]}{\partial x} \{\Phi\} \quad \text{and} \quad \frac{\partial \phi}{\partial y} = \frac{\partial [N]}{\partial y} \{\Phi\}. \tag{10}$$

Let the domain Ω be divided into a finite number of subdomains or elements (triangular) as shown in Fig. 2. Then the integrals over the domain Ω and its boundary $\partial\Omega$ in Eq. (9) can be replaced by the sum of the integrals over the domain, Ω_e, of each element and over the boundary, $\partial\Omega_e$, of each boundary elements. Now using Eqs. (10) and (6) for $D(\partial\phi_s/\partial n)$ in Eq. (9) and writing out the gradient terms,

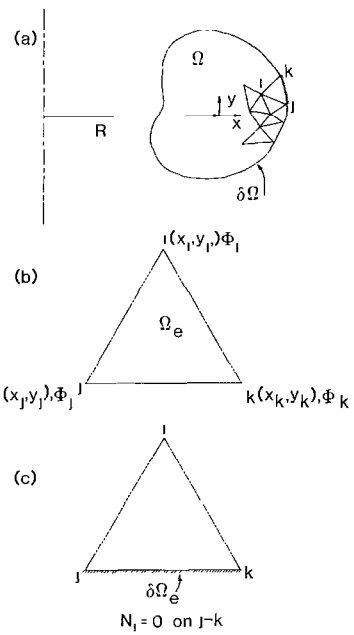

FIG. 2. (a) Discretization of the domain, Ω, into triangular elements. (b) The nodal conditions at the nodes i, j, k. (c) An element with one side belonging to the boundary, $\partial\Omega$.

the finite element equations for a single element, e, for the solution of the group diffusion equation, Eq. (4), in R–Z cylindrical/toroidal coordinates is obtained:

$$
\begin{aligned}
&2\pi \int_{\Omega_e} \frac{1}{(R+x)} \frac{\partial [N]}{\partial x} (R+x)\, D_e \frac{\partial [N]}{\partial x} \{\Phi\}(R+x)\, dA_e \\
&\quad + 2\pi \int_{\Omega_e} \frac{\partial [N]}{\partial y} D_e \frac{\partial [N]}{\partial y} \{\Phi\}(R+x)\, dA_e \\
&\quad + 2\pi \int_{\partial\Omega_e} \frac{1}{2} \left(\frac{1-\alpha}{1+\alpha}\right) [N]^{\mathrm{T}} \phi_s (R+x)\, dL_e + 2\pi \int_{\Omega_e} [N]^{\mathrm{T}} [N]\, \sigma_t \{\Phi\}(R+x)\, dA_e \\
&= 2\pi \sum_{g'=1}^{G} \sigma_{g' \to g} \int_{\Omega_e} [N]^{\mathrm{T}} [N] \{\Phi\}^{g'} (R+x)\, dA_e + 2\pi \int_{\Omega_e} [N]^{\mathrm{T}} S_v^e (R+x)\, dA_e \\
&\quad + 2\pi \int_{\partial\Omega_e} \frac{2S_0^e}{(1+\alpha)} [N]^{\mathrm{T}} (R+x)\, dL_e. \qquad (11)
\end{aligned}
$$

In Eq. (11), expressions for differential volume and surface elements (with toroidal symmetry), $dV_e = 2\pi(R+x)\, dz\, dy = 2\pi(R+x)\, dA_e$ and $dS_e = 2\pi(R+x)\, dL_e$ respectively, have been used. The integrations in Eq. (11) can be evaluated either analytically or numerically depending on the complexity of the known basis functions, $N(x, y)$. When this is done, we obtain an element matrix equation as

$$\mathbf{A}^e \{\Phi\}^e = \{q\}^e, \qquad (12)$$

where $\mathbf{A}^e$ is a square matrix of size $(n \times n)$, n being the number of unknown nodal values in the element, e. Matrix representation for the whole domain Ω and its boundary $\partial\Omega$ is obtained by properly adding Eq. (12) for all the elements in the domain, Ω. To obtain explicit expressions for $\mathbf{A}^e$ and $\{q\}^e$, we need basis functions, $N(x, y)$.

Let the neutral flux ϕ be represented by a linear polynomial in an element, e,

$$\phi = \alpha_1 + \alpha_2 x + \alpha_3 y \qquad (13)$$

with nodal conditions:

$$
\begin{aligned}
\phi &= \Phi_i \qquad \text{at} \quad x = X_i,\ y = Y_i \\
\phi &= \Phi_j \qquad \text{at} \quad x = X_j,\ y = Y_j \\
\phi &= \Phi_k \qquad \text{at} \quad x = X_k,\ y = Y_k.
\end{aligned}
$$

By inserting these conditions in Eq. (13), one finds, α_1, α_2, and α_3. Then ϕ can be written as [25]

$$\phi = [N]\{\Phi\} = N_i \Phi_i + N_j \Phi_j + N_k \phi_k,$$

where the basis functions are

$$N_i = \frac{1}{2A}(a_i + b_i x + c_i y)$$

$$N_j = \frac{1}{2A}(a_j + b_j x + c_j y)$$

$$N_k = \frac{1}{2A}(a_k + b_k x + c_k y).$$

Here, A is the area of the triangular element with vertices i, j, and k read counterclockwise and a, b, and c are constants determined by the nodal coordinates. The integrals in Eq. (11) can be evaluated analytically with linear polynomial in Eq. (13). Use of higher order polynomials would require numerical integration. If the side j–k of an element belongs to the boundary $\partial\Omega$, then the expression for ϕ on this boundary side becomes

$$\phi_s = \phi_{jk} = [N]\{\Phi\} = [0\ N_j\ N_k] \begin{bmatrix} \Phi_i \\ \Phi_j \\ \Phi_k \end{bmatrix},$$

since $N_i = 0$ on j–k, and similarly for the other two sides if they also belong to the boundary.

Inserting these expressions for the basis functions and their derivatives in Eq. (11) and evaluating the line and area integrals, we obtain the expressions for $\mathbf{A}^e$ and $\{q\}^e$ in Eq. (12). For R–Z toroidal/cylindrical geometry, $\mathbf{A}^e$ is given by

$$\mathbf{A}^e = 2\pi\bar{X}\frac{D_e}{4A_e}\begin{bmatrix} b_i^2 & b_i b_j & b_i b_k \\ b_i b_j & b_j^2 & b_j b_k \\ b_i b_k & b_j b_k & b_k^2 \end{bmatrix} + 2\pi\bar{X}\frac{D_e}{4A_e}\begin{bmatrix} c_i^2 & c_i c_j & c_i c_k \\ c_i c_j & c_j^2 & c_j c_k \\ c_i c_k & c_j c_k & c_k^2 \end{bmatrix}$$

$$+ 2\pi\sigma_i^e A_e \begin{bmatrix} d_1 & e_1 & e_2 \\ e_1 & d_2 & e_3 \\ e_2 & e_3 & d_3 \end{bmatrix}$$

$$+ 2\pi\left(\frac{1-\alpha}{1+\alpha}\right)\frac{L_{ij}^e}{24}\begin{bmatrix} (3X_i + X_j) & (X_i + X_j) & 0 \\ (X_i + X_j) & (X_i + 3X_j) & 0 \\ 0 & 0 & 0 \end{bmatrix}, \tag{14}$$

where $\bar{X} = (X_i + X_j + X_k)/3$. The last term in Eq. (14) arises when the side i–j belongs to the boundary, $\partial\Omega$. If the element is not a boundary element, this term

would be absent. If $j-k$ or $k-i$ is the boundary side, then the last term in Eq. (14) would respectively be

$$2\pi\left(\frac{1-\alpha}{1+\alpha}\right)\frac{L^e_{jk}}{24}\begin{bmatrix}0 & 0 & 0\\ 0 & (3X_j+X_k) & (X_j+X_k)\\ 0 & (X_j+X_k) & (X_j+3X_k)\end{bmatrix}$$

or

$$2\pi\left(\frac{1-\alpha}{1+\alpha}\right)\frac{L^e_{ki}}{24}\begin{bmatrix}(3X_i+X_k) & 0 & (X_i+X_k)\\ 0 & 0 & 0\\ (X_i+X_k) & 0 & (X_i+3X_k)\end{bmatrix},$$

where

$$d_1=(3X_i+X_j+X_k)/30 \qquad e_1=(2X_i+2X_j+X_k)/60$$
$$d_2=(X_i+3X_j+X_k)/30 \qquad e_2=(X_i+2X_j+2X_k)/60$$
$$d_3=(X_i+X_j+3X_k)/30 \qquad e_3=(2X_i+X_j+2X_k)/60.$$

L^e_{ij}, L^e_{jk}, and L^e_{ki} are the lengths of the respective side of the triangular element, e, and $\{q\}^e$ is given by

$$\{q\}^e=2\pi\sum_{g'=1}^{G}\sigma_{g'\to g}A_e\begin{bmatrix}d_1 & e_1 & e_1 & \Phi_i\\ & d_2 & e_3 & \Phi_j\\ \text{sym.} & & d_3 & \Phi_k\end{bmatrix}^{g'}+2\pi S^e_i A_e\begin{bmatrix}u_1\\ u_2\\ u_3\end{bmatrix}$$

$$+2\pi S^e_0 L^e_{ij}\begin{bmatrix}\frac{X_i}{3}+\frac{X_j}{6}\\ \frac{X_i}{6}+\frac{X_j}{3}\\ 0\end{bmatrix}. \tag{15}$$

If $j-k$ or $k-i$ is the boundary side, then the last term in Eq. (15) would respectively be

$$2\pi S^e_0 L^e_{jk}\begin{bmatrix}0\\ \frac{X_j}{3}+\frac{X_k}{6}\\ \frac{X_j}{6}+\frac{X_k}{3}\end{bmatrix}$$

or

$$2\pi S_0^e L_{kl}^e \begin{bmatrix} \frac{X_l}{3}+\frac{X_k}{6} \\ 0 \\ \frac{X_i}{6}+\frac{X_k}{3} \end{bmatrix},$$

where

$$u_1=(2X_l+X_j+X_k)/12$$
$$u_2=(X_l+2X_j+X_k)/12$$
$$u_3=(X_l+X_j+2X_k)/12.$$

It can be seen from Eq. (14) that the element matrix $\mathbf{A}^e$ is symmetric, diagonally dominant, and positive definite. When the Eqs. (14) and (15) are properly summed over all the elements in the domain Ω, we obtain the global matrix representation of the nodal values of the neutral flux, Φ,

$$\mathbf{A}\{\Phi\}=\{q\}. \tag{16}$$

The global matrix evidently has the above-mentioned properties. In the next section we discuss the solution of the matrix Eq. (16) and general characteristics of the code, FENAT, which is based on this solution.

IV. Solution of the Finite Element Equations

An equation similar to Eq. (16) exists for each energy group. These equations are coupled through the right-hand side $\{q\}$ which contains the charge-exchange (scattering) source term. At each iteration over the energy groups, the right-hand side $\{q\}$ for each group must be recalculated from the most recent group fluxes. The global matrix $\mathbf{A}$ is fixed for a specific discretization of the domain Ω. Hence, we have, for each energy group, a matrix equation where the matrix $\mathbf{A}$ is fixed but the right-hand side is changing. Since the matrix $\mathbf{A}$ is diagonally dominant and positive definite, convergence and stability of the solution of Eq. (16) is guaranteed. The matrix $\mathbf{A}$ is banded and sparse. The bandwith depends on the problem size and the way of numbering the nodes.

There are two major groups of methods for solving this set of equations. These are the direct or elimination methods and the iterative methods. A survey of available elimination and iterative methods is available elsewhere [25–29]. It is a unanimous view in the structural mechanics community that the iterative methods cannot compete with the elimination methods, especially for problems with multiple

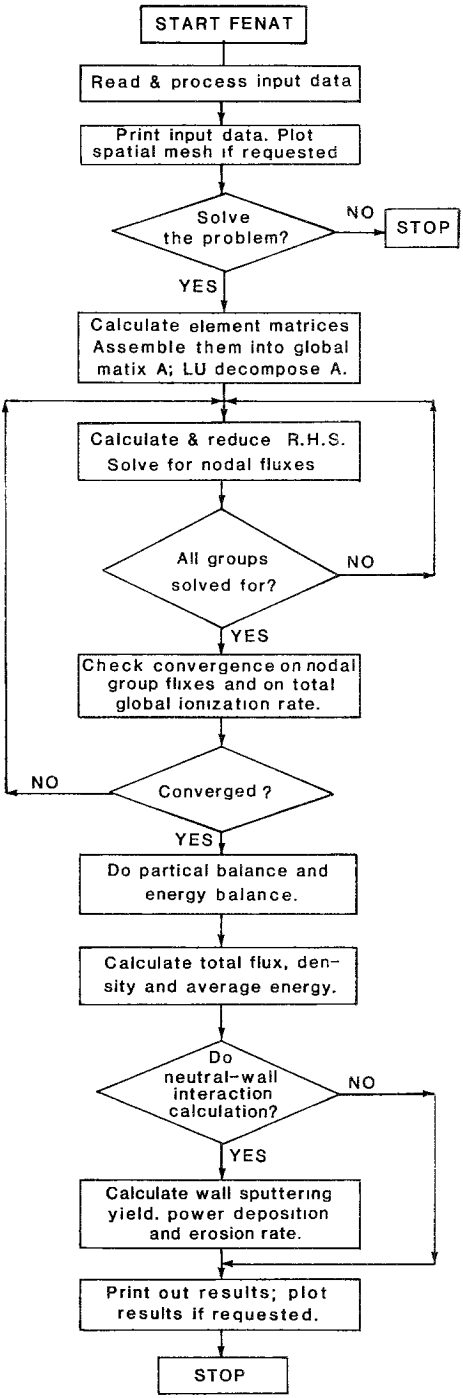

FIG 3. A simplified logical flow diagram for FENAT.

right-hand sides [25–27]. As mentioned above, the right-hand side of Eq. (16) changes because of the charge exchange source term in it. Therefore, an elimination method has been selected to solve the set of Eq. (16). This method is based on the column profile storage of the global matrix **A** and its L–U decomposition by Crout variation of Gauss elimination [27].

The use of a linear polynomial for the basis functions gives a convergence rate of order, $O(h^2)$, where "h" is the size of an element. Therefore, if the element size is halved, the discretization error in Φ will be reduced to one-fourth. In the case of neutral atom transport, "h" should be smaller than the mean free path near sources or in regions of rapid flux variation to make the discretization error negligible. In regions where Φ varies slowly, the element size can be equal to, or even larger than, the mean free path. Decreasing the mesh spacing by half will increase the number of nodal points to about four times and hence the computation time. If the mesh size is selected judiciously using the above guideline, the results will be highly accurate. Convergence is checked after each iteration (n) on the group fluxes (Φ) at each node (i) and on the global ionization or absorption rate (I), that is, by

$$\frac{|\Phi_i^{n+1} - \Phi_i^n|}{\Phi_i^n} \leqslant \varepsilon_1 \qquad \text{and} \qquad \frac{|I^{n+1} - I^n|}{I^n} \leqslant \varepsilon_2. \tag{17}$$

Iteration is terminated whenever any of the above conditions is satisfied.

The code we have developed based on this solution method is called FENAT, an acronym for finite element neutral atom transport. It is written for use on CRAY computers. Solution can be obtained in X–Y cartesian and R–Z cylindrical/toroidal geometries. Dynamic memory allocation is provided. Hence, small problems will require short clock-time for running. Various plotting options such as spatial mesh plot in its entirity or in a specified number of windows, 3D total neutral atom flux, density and average energy plots, variation of total density and average energy as functions of poloidal angle and plasma radii as parameters, contour plot of total density, and plots of wall-material sputtering, erosion rate and power deposition as functions of poloidal angle are provided. Figure 3 is a simplified flow chart for FENAT. Detailed information for running the code is provided in a user's manual [30].

V. Verification of FENAT and Its Application to TEXTOR Tokamak

Accuracy of FENAT has been assesed by comparing it with the two-dimensional transport theory code DOT-4.3 [13]. Figure 4 compares the results of FENAT with those of DOT-4.3. The problem is a 20 by 20 cm square plasma in cartesian coordinates. Neutrals at the top, bottom, and right surface are reflected while the left surface is subject to a vacuum boundary condition. A surface source of neutrals is localized at $x = 20$ cm and $y = 8$–14 cm. In Fig. 4a, the medium is homogeneous with the scattering to total cross section ratio, c, equal to 0.8 and the mean free

path is 4 cm. This is a one-group solution. In Fig. 4b, the medium is plasma with the following properties:

$$T_i(0) = T_e(0) = 1 \text{ KeV}$$

$$T_i(20) = T_e(20) = 50 \text{ eV}$$

$$n_i(0) = n_e(0) = 5 \times 10^{13} \text{ cm}^{-3}$$

$$n_i(20) = n_e(20) = 1 \times 10^{12} \text{ cm}^{-3}$$

energy of source neutrals, a few eV.

Plasma properties are uniform along y. Temperature and density profiles are assumed parabolic. The flux in Fig. 4a and total density in Fig. 4b are shown as functions of x at $y = 2$ cm and $y = 10$ cm. Figure 5 compares the total neutral density by FENAT and DOT-4.3 for R–Z toroidal geometry with 20 by 20 cm square cross section. The boundary and source conditions and the plasma properties are similar to those in Fig. 4b. Both Figs. 4 and 5 show that FENAT is quite accurate

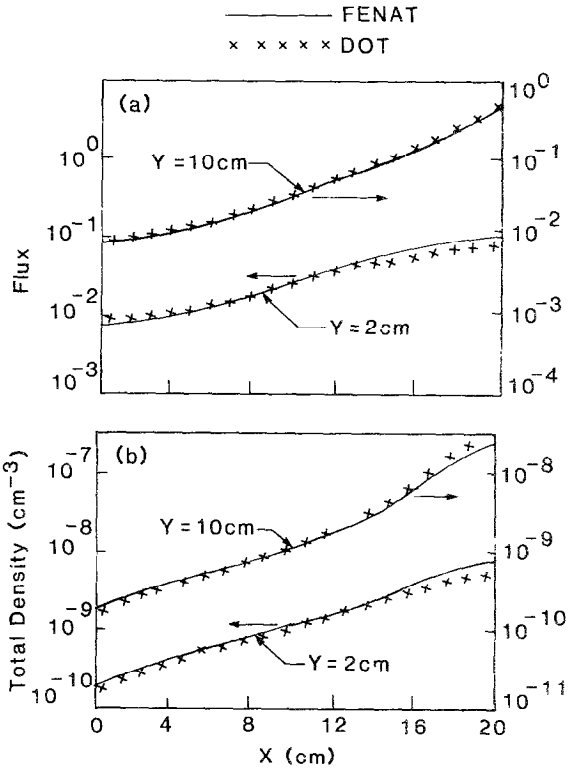

FIG. 4. Comparision of neutral flux ($\text{cm}^{-2}\text{s}^{-1}$) and total neutral density by DOT-4.3 and FENAT for 2D X–Y geometries. DOT to FENAT CPU time ratio is about 4 in case (a) and about 62 in case (b)

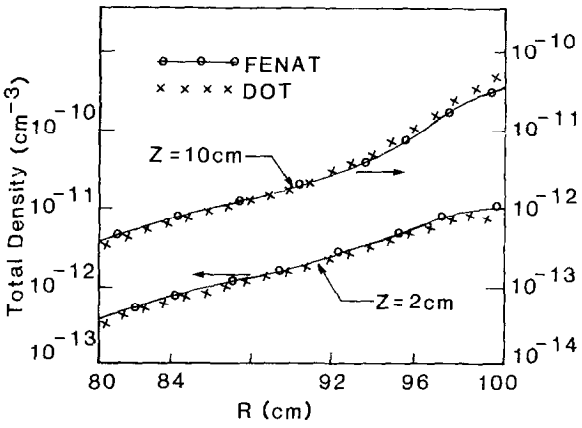

FIG. 5. Comparison of total neutral atom density by FENAT and DOT-4.3 for 2D R–Z toroidal geometry. DOT to FENAT CPU time ratio is about 96.

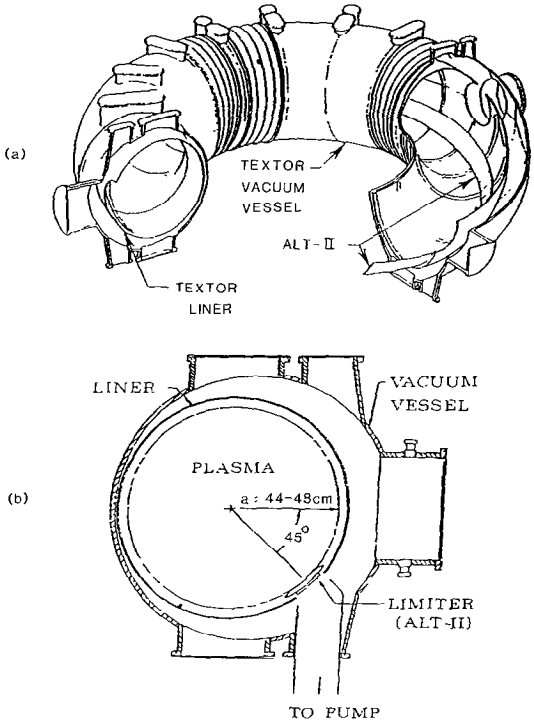

FIG. 6. TEXTOR geometry with ALT-II limiter: (a) cutaway view of the TEXTOR vessel; (b) TEXTOR cross section showing the location of the limiter, ALT-II.

compared to the transport theory. For the cases in Figs. 4b and 5, FENAT is about 62 and 96 times faster than DOT-4.3, respectively. It appears that the transport theory code converges rather slowly when there is complete up-scattering and down-scattering in the multigroup cross section as is the case for plasma-neutral interactions.

FENAT has been applied to calculate the distribution of limiter-originated neutral atoms in the TEXTOR tokamak plasma [31]. Figure 6 shows the TEXTOR geometry. Figure 6a shows a cutaway view of the vacuum vessel with the toroidal belt limiter, ALT-II [18] in place. Figure 6b shows a cross-sectional view of the vacuum vessel. The limiter is located in the fourth quadrant centered at 45° and is a localized source of neutral atoms due to the recycling of neutralized plasma ions from the limiter surface. The neutral source is 20 times larger at the limiter tips than at the rest of the limiter surface. Table I contains the TEXTOR parameters and the plasma properties. The reflection coefficients are calculated from Ref. [32]. All neutral atoms not reflected directly from the wall are assumed to desorb and reenter the plasma with a few eV of energy. Fifteen energy groups up to the maximum energy of 3 keV have been used.

Figure 7 shows the spatial mesh plotted in four windows. The boundary elements marked by "*s*" represent the limiter (surface source). Total neutral atom density is shown in the 3D plot in Fig. 8. The two peaks correspond to the tips of the limiter. A 3D plot of average neutral energy is shown in Fig. 9. Figure 10 shows the average energy plotted as a function of poloidal angle at five plasma radii. Figures 9 and 10 show that the average energy of the neutral atoms is low near the plasma edge and higher and flat towards the center of the plasma. This is due to the well-known fact that plasma acts as a filter for low energy neutrals so that the energy spectrum of neutral atoms becomes harder as one proceeds towards the center of the plasma. The plasma is optically thin for high energy neutrals. In this problem, there are

TABLE I

TEXTOR Parameters and Plasma Properties

Major radius	175 cm
Minor radius	48 cm
Plasma cross section	Circular
Limiter material	Graphite
First-wall material (assumed iron)	Stainless steel
Central plasma ion temperature	0.773 keV
Central plasma electron temperature	0.865 keV
Edge plasma ion temperature	50 eV
Edge plasma electron temperature	100 eV
Central plasma density	2.5×10^{13} cm^{-3}
Edge plasma density	8.4×10^{12} cm^{-3}
Total plasma ion efflux rate	6.0×10^{21} s^{-1}

Note. Parabolic temperature and density profiles are assumed.

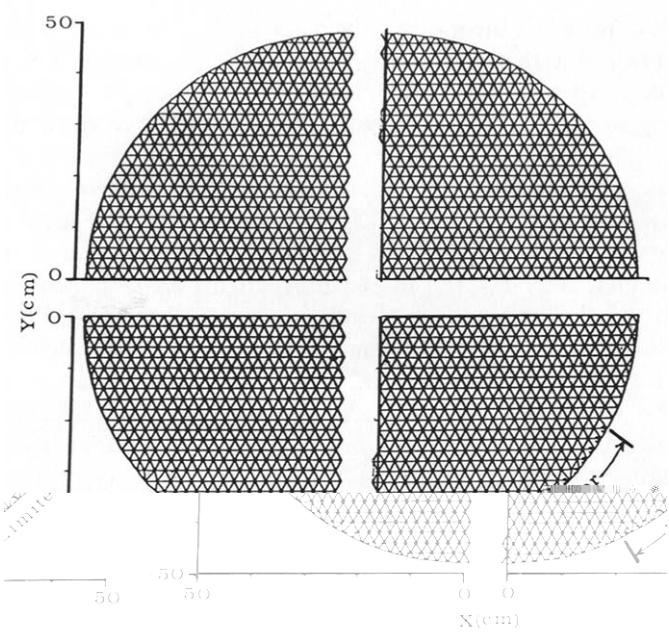

FIG. 7. FENAT spatial mesh for TEXTOR geometry. The mesh is plotted in 4 windows. Elements marked by "s" represent the limiter (surface source).

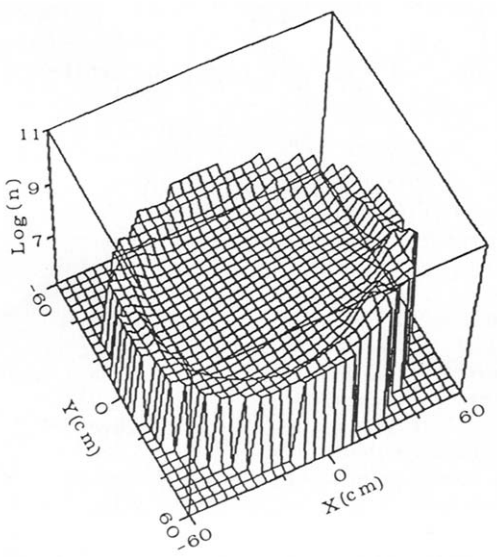

FIG. 8. 3D plot of total neutral atom density in TEXTOR by FENAT. The maximum total density is normalized to $10^{10}\,cm^{-3}$.

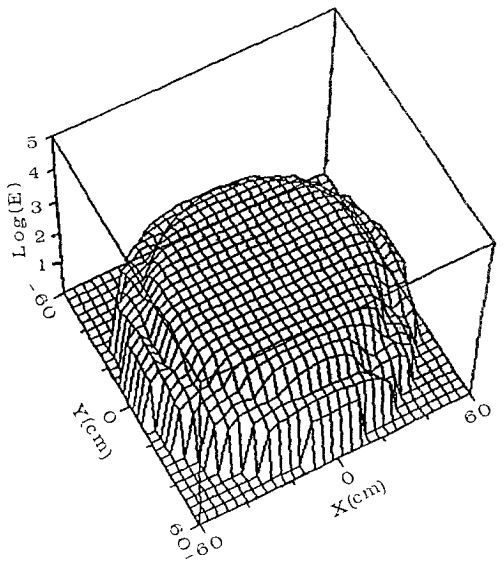

FIG. 9. 3D plot of average neutral atom energy (eV) in TEXTOR by FENAT. Low energy near the edge is due to the filtering of the wall-originated low energy neutral atoms by the plasma towards the plasma edge.

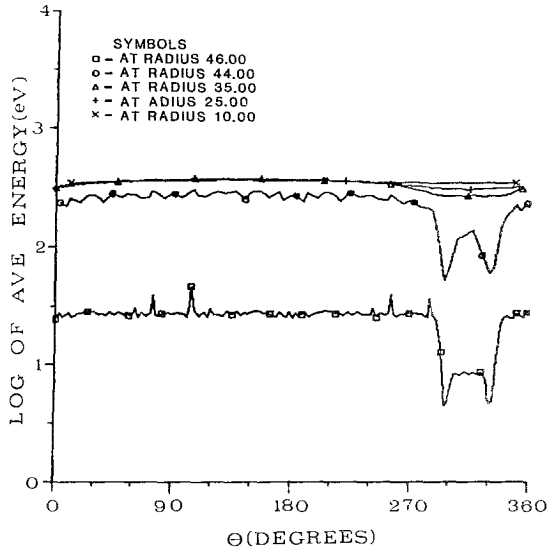

FIG. 10. Variation of average neutral atom energy along the poloidal direction at five plasma radii. The limiter is located between 297 and 333°

1886 nodal points (unknowns), 3640 triangular elements, and 15 energy groups. The computation time is about 2 min on the CRAY-1 (D-Machine).

It is useful to examine the breakup of computation time for the TEXTOR problem. Reading, printout, and processing of the data and the calculation of element matrices required about 2s. The entire mesh plot in 4 windows required about 4s. L–U decomposition of the 15 global matrices (one for each energy group) by Crout elimination took nearly 18s. About 4s were required per iteration over the 15 energy groups. With a starting flux guess of zero, 26 iterations were needed to meet the convergence criterion of $\varepsilon_1 = 10^{-4}$ (giving a particle balance, loss to source ratio, of 0.9999926) and 15 iterations were needed for $\varepsilon_1 = 10^{-2}$ (balance = 0.9988).

In a plasma simulation, plasma temperature and density evolve gradually. In this case, the neutral flux for the previous plasma profiles is a good guess for the new plasma profiles. Only a few iterations are needed for convergence. Consequently, the computation time will be much shorter than 2 min ($\varepsilon_1 = 10^{-4}$, 26 iterations) or 1.4 min ($\varepsilon_1 = 10^{-2}$, 15 iterations) for the above TEXTOR problem when FENAT is used as part of an overall plasma simulation. Again for the TEXTOR problem, we have probably used more than the optimum number of energy groups and smaller element size than required for adequate accuracy. The computation time is directly proportional to the number of energy groups used.

Since multidimensional neutral atom transport is at present calculated by Monte Carlo codes, we provide a rough comparison between FENAT and Monte Carlo codes. FENAT will compare favorably in both speed and accuracy with the Monte Carlo code SEURAT [33]. The Monte Carlo code DEGAS resuired 2–5 min of CRAY-1 time for a neutral calculation in a 33 by 50 cm edge plasma and gives a maximum error of 15% (standard deviation) [34]. FENAT will require less than half a minute for this problem. We note that the 5-group neutral solution in the 20 by 20 cm plasma in Fig. 5 requires only 3s to meet the convergence criterion of $\varepsilon_1 = 10^{-4}$.

In all of the results presented in this paper, the plasma properties and hence the group cross sections are functions of one coordinate only. Computation time required by FENAT will not change if the cross sections vary along both coordinates. Additional memory may be required if the user employs more cross-section sets to represent the variations of plasma properties in two coordinates. Note that FENAT in its present form is neither fully vecotrized nor optimized. An order of magnitude reduction of computation time in FENAT can be expected by optimizing the code using vectorization, parallel processing, and local memory allocation simultaneously.

VI. Summary and Conclusions

A two-dimensional code, FENAT, for the transport of neutral atoms in fusion plasmas has been developed based on the solution of the multigroup diffusion equation using the finite element Galerkin method. Geometries allowed are X–Y

cartesian and R–Z cylindrical/toroidal. FENAT can handle noncricular cross-section plasmas such as D-shaped or any other complicated cross section. Mesh data generation is not fully automatic at this stage. However, because of the semi-automatic mesh data generation, the actual amount of information to be supplied by the user is much less than the total amount of data. In a large, high density plasma, the volumetric source of neutral atoms due to recombination may become significant. FENAT can handle both boundary and volume sources equally well [16]. In its present form, FENAT requires that any volumetric source as well as boundary source be supplied by the user in the input data. However, with a minor modification, a recombination source can be calculated internally from the plasma density and temperature distributions. Comparison with the transport theory code DOT-4.3 has shown that FENAT is accurate and much faster than DOT-4.3. FENAT will be faster and give better accuracy than Monte Carlo codes.

Localized neutral atom sources, such as limiter-originated neutrals in tokamak problems, lead to neutral atom density and wall effects that are strong functions of poloidal angle. In such cases, results from one-dimensional (slab or cylindrical) solutions of neutral atom distribution will be inadequate. Neutral atom distributions from a 2D or 3D neutral atom transport code can be used in plasma simulation codes such as WHIST [3] or BALDUR [4]. The use of diffusion theory will yield accurate solutions with considerably greater speed. The FENAT code is the first step in this direction and can be used in conjunction with two-dimensional plasma modelling codes.

ACKNOWLEDGMENTS

We acknowledge the use in FENAT of several subroutines, after some modification, from Ref [27]. The code PLASMX was obtained from RSIC, Oak Ridge National Laboratory. This work was supported by the U.S. DOE, Office of Fusion Energy under Contract DE-FG03-86ER52130

REFERENCES

1. S. REHKER AND H WOBIG, *Plasma Phys.* **15**, 1083 (1973).
2. T. F. VOLKOV AND Y. L. IGITKHANOV, *Sov. J. Plasma Phys.* **3**, 668 (1977).
3. W. A. HOULBERG AND R. W. CONN, *Nucl. Sci Eng.* **64**, 141 (1977).
4. D. POST *et al.*, TFTR Physics Group Report No. 33, Princeton University, Plasma Physics Laboratory, Princeton, NJ, 1981 (unpublished).
5. K. H. BURRELL, *J. Comput. Phys.* **27**, 88 (1978).
6. K. AUDENAERDE, G. A. EMMERT, AND M. GORDINIER, *J. Comput. Phys* **34**, 268 (1980).
7. M. W HUGHES AND D. E. POST, *J. Comput. Phys.* **28**, 43 (1978).
8. D. F. DUCHS, D. E POST, AND P H. RUTHERFORD, *Nucl. Fusion* **17**, 565 (1977).
9. R D. GARCIA, G C. POMRANING, AND C. E. SIEWERT, *Plasma Phys.* **24**, 903 (1982).
10. D. HEIFETZ, D. POST, M. PETRAVIC, J. WEISHEIT, AND G. BATEMAN, *J. Comput. Phys.* **46**, 309 (1982).
11. D. REITER AND A. NICOLAI, *J. Nucl. Mater.* **128/129**, 458 (1984)
12. W W ENGLE JR., *A User's Manual for ANISN, A One-Dimensional Discrete Ordinates Transport*

13. W. A. RHOADES AND R. L. CHILDS, *An Update Version of DOT4 One- and Two-Dimensional Neutron/Photon Transport Code*, ORNL-5851 (Oak Ridge National Laboratory, April, 1982); CCC-429 (Radiation Shielding and Information Center, 1982).
14. T. J. SEED, W. F. MILLER, AND F. W. BRINKLEY, Los Alamos Scientific Laboratory Report LA-6735-MS, 1977 (unpublished).
15. J. H. MARABLE AND E. M. OBLOW, *Nucl. Sci. Eng.* **61**, 90 (1976).
16. M. Z. HASAN, R. W. CONN, AND G. C. POMRANING, *Nucl. Fusion* **27**, 117 (1987).
17. M. Z. HASAN, Ph. D. dissertation, University of California, Los Angeles, 1985 (unpublished).
18. R. W. CON *et al.*, *J. Nucl. Mater.* **121**, 350 (1984).
19. G. I. BELL AND S. GLASSTONE, *Nuclear Reactor Theory* (Krieger, Huntington, NY, 1977).
20. J. J. DUDERSTAQDT AND L. J. HAMILTON, *Nuclear Reactor Analysis* (Wiley New York, 1976).
21. PSR-106, RSIC, Oak Ridge National Laboratory, 1977.
22. G. ARFKEN, *Mathematical Methods for Physicists* (Academic Press, New York, 1970).
23. G. C. POMRANING AND C. A. STEVENS. *Nucl. Sci. Eng.* **55**, 1974
24. G. FAIRWEATHER, *Finite Element Galerkin Methods for Differential Equations* (Dekker, New York/Basel, 1978).
25. L. J. SEGARLIND, *Applied Finite Element Analysis* (Wiley, New York, 1976)
26. E. SCHREM, *Numerical & Computer Methods in Structural Mechanics* (Academic Press, New York, 1973).
27. O. C. ZIENKIEWICZ, *The Finite Element Methods*, 3rd ed. (McGraw–Hill, London, 1977).
28. D. K. FADDEEV AND V N. FADDEEVA, *Computational Methods of Linear Algebra* (Freeman, San Francisco, 1963).
29. D. S. KERSHAW, *J. Comput. Phys.* **26**, 43 (1978).
30. M. Z. HASAN, UCLA Center for Plasma Physics and Fusion Engineering Report PPG-917, 1986 (unpublished).
31. UCLA Report, UCLA-ENG-8405, PPG-755, 1985 (unpublished).
32. W. ECKSTEIN AND H. VERBEEK, *Data on Light Ion Reflection* (Max-Planck Institute of Plasma Physics, Garching bei Munich, West Germany, 1979).
33. D. B. HEIFETZ AND D. E. POST, *Comput. Phys. Commun.* **29**, 287 (1983).
34. D. B HEIFETZ, Plasma Physics Laboratory, Princeton University, Princeton, NJ, private communication, 1986.